

NUMERICAL SIMULATION OF THE RD-14M TEST T9308

M. An^{*}, W. Thompson^{*}, and M. Wright^{**}

ABSTRACT

The transient two-phase flow field within outlet header #5 of RD-14M during the thermosyphoning test T9308 has been numerically simulated. The analysis is focused on the role of the header flow conditions in two unexpected observations during this thermosyphoning test, namely, flow reversal in the channels of heated sections 11 and 12, and flow stalling and subsequent heat-up of the fuel element simulator in heated section 11. While the work reported herein is preliminary in nature, it appears that at all times during the transient there was a significant amount of stratified water in the header. Further, it appears that the reduced-scale nature of the RD-14M facility, involving only 5 connected “feeders” is such that localised conditions occur within the header, that may play a role in the conditions observed. It is believed that such localised conditions could not occur in a full-size CANDU header.

1. Introduction

In 1990, the AECB opened Action Item 90G02 to track the progress of Canadian nuclear utilities in addressing concerns related to core cooling in the absence of forced flow. The AECB was concerned that, under thermosyphoning conditions in the unbroken loop following a LOCA, flow may stop in individual channels, leading to high sheath temperatures, which may jeopardise the integrity of the unbroken loop pressure boundary and escalate the consequences of the initial event. This type of flow behaviour occurred in a few thermosyphoning experiments performed with the RD-14M facility [1] at a relatively high system inventory. The percentage of inventory in the loop at this time was comparable to that in an unbroken loop in the reactor following a LOCA.

Over the intervening years, many simulations of the RD-14M experiments have been performed in which thermosyphoning flow breaks down. Recently, simulations of one test, T9308 [2], have shown that individual heated section (HS) behaviour is best matched with various two-phase conditions at each feeder connection to the outlet header. However, the header conditions in these CATHENA simulations were treated as reservoirs at experimental pressures, and trial and error was used to determine the transient void conditions at the feeder connections. A fundamental assessment of the header fluid conditions is therefore required to confidently predict the reactor situation.

* Atlantic Nuclear Services Ltd., Fredericton, New Brunswick

** Wright Analytic, Saint John, New Brunswick

Two unexpected flow conditions occurred during the T9308 test. Flows reversed in the channels for HS11 and HS12 at around 17600 seconds, and the fuel element simulator (FES) in HS11 started to heat up at around 20900 seconds due to flow stalling, which terminated the experiment. In this paper we investigate the role of outlet header #5 in creating these occurrences by simulating the transient 3-D behaviour of the water-steam mixture within the outlet header during the test.

2. Geometry Model

The geometry of outlet header #5 is shown in Figure 1. Connected to the header are five outlet feeders from heated sections 10 to 14, one boiler pipe rising to boiler #1, and one dead-end pipe connected to the pressure relief valve. The outlet feeders from HS10, HS12, and HS14 (from the right) intersect with the front Y-Z plane, while those from HS11 and HS13 (from the right) intersect with the bottom X-Y plane. The presence of the pressure relief valve is not representative of a CANDU reactor, but is required for over-pressure protection of the RD-14M test-rig. Along with other minor modifications to the original AutoCAD-generated geometry from AECL-WRL [3], the dead-end pipe has been “pulled in” axially to one end of the header in the Y direction to save computer resources while conserving the volume and height of the original pipe. This pipe may be important during the transient process for refilling the header due to its contained volume and height relative to the header.

The total dimension of the final geometry is 0.668 m x 0.990 m x 0.647 m in the X, Y, and Z co-ordinate directions, respectively (Figure 1). This geometry model includes some pipe components with small diameters and degrees of inclination that require fine resolution. Therefore, the non-uniform grid generation over the computational domain encompassing the geometry has led to a large number of cells, i.e., 42 x 59 x 43 in the X, Y, and Z directions, respectively. As a result, considerable CPU time was required for one transient simulation step.

3. Simulation Time Periods

The T9308 test lasted more than 21700 seconds. Because of time and resource restraints, the transient simulation could only be started before the first flow reversal in HS12 during the test. However, the initial field for transient simulation was obtained on the assumption that the steady state at this starting time was sufficiently ahead of the first flow reversal that the effect of the steady-state initial field on the transient solutions prior to flow reversal was negligible.

The starting time was selected by analysing the boundary conditions applied to the outlet feeders, which reflect the flow behaviours in the channels during the test. CATHENA predictions were used for these boundary conditions [4] because of the lack of available measurements. For this purpose, AECL was requested to reproduce the CATHENA

results reported in TTR-642 [2] with a uniform void, which had a time variation as defined in Section 3.3.1 of TTR-642 and which was applied at all five outlet feeder ports for 20700 seconds, prior to flow stalling in HS11. After 20700 seconds, the feeder port for HS11 was specified as having a different void variation, as prescribed in Section 3.3.2 of TTR-642, in order to fit the measured FES heat-up in HS11. The other four ports were assumed to have the same void, which varied with time according to Section 3.3.1 of TTR-642. CATHENA had predicted that the flow reversal would occur at about 17100 seconds, which was about 500 seconds ahead of the experimental observation. Since the CATHENA results were used as boundary conditions, the transient simulation was launched at 17000 seconds.

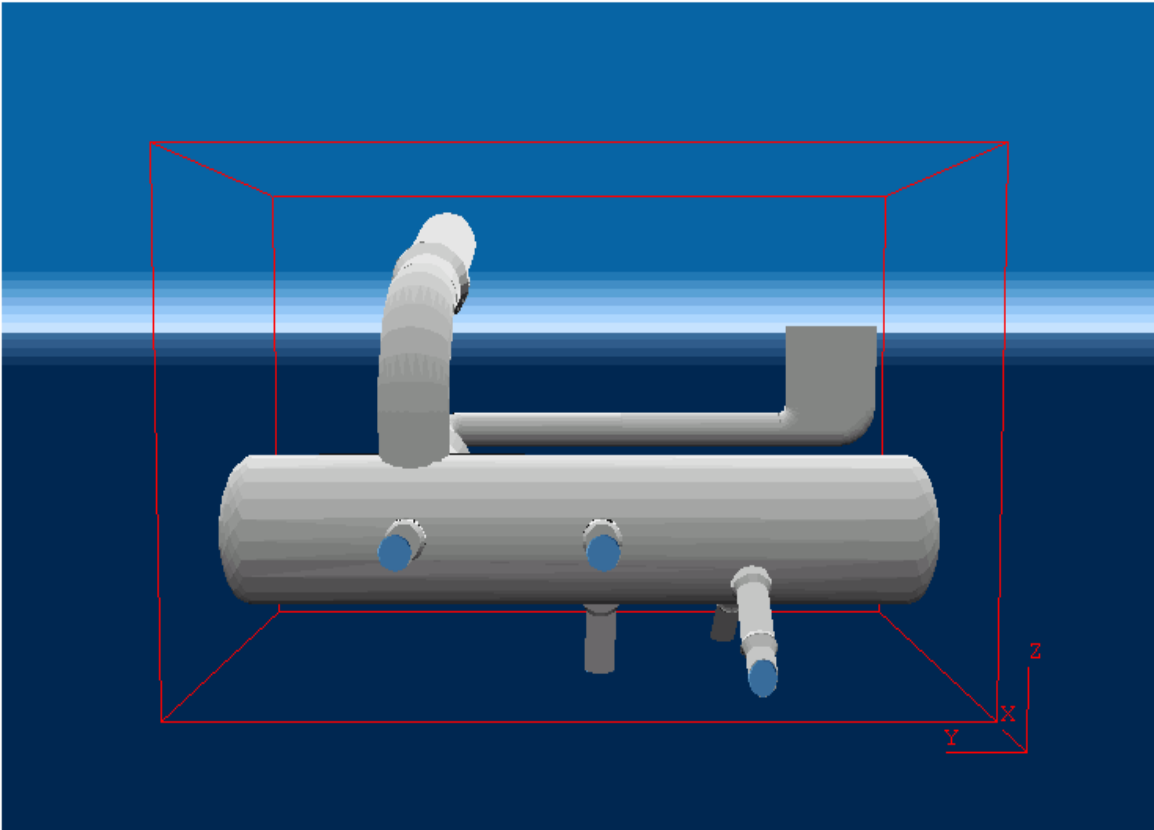


Figure 1. The geometry model

The transient simulation was divided into three time periods. The first stage, covering the time period 17000 seconds to about 17124 seconds, examined in detail the header flow

conditions around the occurrence of the flow reversal. The second stage covered a transition period from 17124 seconds to 20724 seconds prior to flow stalling in HS11. This was designed to check for any fluid refilling from the dead-end pipe into the outlet header during this relatively long period, and to obtain an initial field for the next simulation period. The third stage focused on the flow conditions within the header around the flow stalling in HS11 from 20724 seconds to 21010 seconds. The computational time-steps used for the first, second, and third simulation periods were 4 seconds, 600 seconds, and 26 seconds, respectively. Time step independence of the predicted results was tested for the second simulation period.

4. Governing Equations

The general purpose Computational Fluid Dynamics (CFD) code, PHOENICS [5], was employed for the simulations. The Eulerian-Eulerian technique which treats the liquid and steam phases as “interpenetrating continua”, was used to determine the relevant variables for each phase, which included pressure, three velocity components, volume fraction, enthalpy, and turbulence. The governing conservative equations averaged over time of within-phase mass, momentum, and energy transport for each phase have the following general form:

$$\frac{d(R_i \rho_i \phi_i)}{dt} + \nabla \cdot (R_i \rho_i \vec{V}_i \phi_i - R_i \Gamma_{\phi,i} \nabla \phi_i) = R_i S_{\phi,i} \quad (4.1)$$

where

t = time,

R_i = volume fraction of phase i,

ρ_i = density of phase i,

ϕ_i = any conserved property of phase i,

\vec{V}_i = velocity vector of phase i,

$\Gamma_{\phi,i}$ = exchange coefficient of the entity ϕ in phase i, and

$S_{\phi,i}$ = source rate of ϕ_i .

Here, $i = 1, 2$ for the liquid water and steam phases, respectively. If $\phi_i = 1$, Equation (4.1) reduces to the mass continuity equation with R_i as the solved-for variable in the equation. The sum of R_i in the mixture should be equal to one. If $\phi_i = U_{j,i}$ where $j = 1, 2, 3$ for the three velocity components, Equation (4.1) becomes the momentum equations in the three co-ordinate directions, since velocity itself can be considered as the momentum per unit mass. If $\phi_i = H_i$, Equation (4.1) will be the energy equation, from which the solved enthalpy H_i , the temperature T_i of phase i, can be inferred. Up to now, there are five equations for the five variables R_i , H_i , and $U_{j,i}$ for each phase. There is no apparent equation for the pressure P_i , but it can be deduced from the continuity and momentum equations during discretisation of the differential equations [6]. It is assumed that both

phases share the same pressure that is derived from the continuity and momentum equations for both phases. Buoyancy force is applied on the momentum equation of the second or steam phase.

The effective viscosity hypothesis is adopted, where the turbulence effect on the mean flow, due to the correlation between the fluctuating velocities and the ϕ 's, is interpreted as a turbulent viscosity in addition to the laminar viscosity of the fluid. Therefore, the exchange coefficient in Equation (4.1) becomes an effective one that is expressed by the following:

$$\Gamma_{\phi,i} = \rho_i \left(\frac{\nu_{l1}}{\text{Pr}_{l\phi,i}} + \frac{\nu_{t1}}{\text{Pr}_{t\phi,i}} \right) \quad (4.2)$$

where

ν = the kinematic viscosity,
 Pr = the Prandtl number,
 l = the laminar value, and
 t = the turbulent value.

The viscosity is assumed to be a property of phase 1 in PHOENICS, and ν_{l1} and ν_{t1} are shared by both phases. Therefore, both laminar and turbulent Prandtl numbers equal one for the momentum equations of both phases. For all other equations of both phases, the turbulent Prandtl numbers, $\text{Pr}_{t\phi,i}$, are 0.9.

This study involved complicated solid-wall orientations forming various small spaces within the computational domain. Therefore, a PHOENICS unique zero-equation turbulence model, LVEL, was selected to determine the turbulent kinematic viscosity ν_t . This model is suitable for situations in which fluid flows through spaces cluttered with many solid objects. In such cases, the grid density between nearby solids is often too coarse for any advanced turbulence models, such as the k- ϵ two-equation model, to be meaningfully employed. The turbulent kinematic viscosity was calculated via Spalding's law of the wall [6], which covers the entire laminar and turbulent regimes of the flow. Thus,

$$\nu_t = \frac{k}{E} \left[e^{X^+} - \sum_{i=0}^4 (X^+)^{i/i!} \right] \quad (4.3)$$

where

$k = 0.41$ and
 $E = 8.6$.

The local parameter X^+ was determined iteratively from a non-linear expression involving k , E , and the local Reynolds number, which is based on the typical local velocity and the normal distance to the nearest wall $WDIS$. The parameter $WDIS$ was calculated from an algebraic function of a scalar variable L and its gradient [6], while L itself was obtained by solving the following:

$$\nabla^2 L = -1 \quad (4.4)$$

with L fixed to zero in solids.

The phase diffusion source terms, representing the turbulent fluxes associated with the correlation between fluctuating velocity and volume fraction, on all the governing equations of the mean two-phase flow, have the following form:

$$\nabla \cdot (\rho_i \Gamma_{R_i} \phi_i \nabla R_i) \quad (4.5)$$

The phase diffusion coefficient Γ_{R_i} is calculated from

$$\Gamma_{R_i} = \frac{V_{t1}}{Pr_{tR_i}} \quad (4.6)$$

where

Pr_{tR_i} = the turbulent Prandtl number for the volume fractions, which was given the value 0.9.

The condition $Pr_{tR_1} = Pr_{tR_2}$ was enforced by PHOENICS for reasons of volume conservation.

The Inter-Phase Slip Algorithm (IPSA) built into PHOENICS was adopted, where the links between the phases — interphase mass, momentum, and heat transfer — have all been introduced via relevant interphase sources in the governing equations for the relevant variables during preliminary test simulations with a simplified geometry. However, due to difficulties of convergence with the actual complicated geometry and time restraint for this work, only the interphase momentum transfer was eventually considered. This simplification in physical mechanism is considered acceptable, since the sole cause for the interphase mass and heat transfers in this case is the variation of pressure, which exhibits little significant change within the whole domain and over the three time periods selected for transient simulations.

Therefore, for phase i momentum equations, the interphase source reduces to that for direct bulk-to-bulk transfer using the following:

$$S_{IP\phi,i} = f_{IP} (\phi_j - \phi_i) \quad (4.7)$$

where

j = the other phase in the mixture.

The interphase drag coefficient, f_{IP} , is expressed as

$$f_{IP} = C_{FIPS} \rho_1 R_1 \text{MAX}(R_2, R_{Low}) \text{VOL} \quad (4.8)$$

where

VOL = the cell volume and

R_{Low} = a small positive number (1.0E-6) used to prevent the interphase friction from vanishing numerically when the volume fraction of phase 2 approaches zero.

Equation (4.8) assumes that the liquid water, i.e., the first phase, is always present in the system and has a finite volume fraction. This has reasonable consequences when friction is concerned, as it ensures that very small bubbles travel at the same velocity as the carrying liquid. The value of the constant C_{FIPS} is problem-specific. In the work reported herein, a C_{FIPS} value of 100 was used.

Since the interphase mass and energy transfers are not considered, it is no longer necessary to solve the energy equations for the two-phase flow within the insulated system. The phase densities are assigned the average value corresponding to the average pressure over each transient simulation period. Pressure varies in the ranges of 1.50 to about 1.55 MPa, 1.50 to about 2.00 MPa, and 1.75 to about 2.00 MPa over the three simulation time periods, respectively, as defined in Section 3.

The boundary condition at the outlet to the boiler was set as a fixed pressure, as derived from the T9308 measurement [7], with the help of information on instrumentation contained in the RD-14M facility documentation [1]. Due to the lack of experimental data, CATHENA predictions reproduced by AECL [4], following TTR-642 [2], as described in Section 3, were used as the boundary conditions at the outlet feeders. Since the CATHENA void and velocity data contained very high frequency noise, it was denoised using the wavelet denoising technique implemented in the ANSL (Atlantic Nuclear Services Ltd.) software Plant Analysis Workbench (PAW) [8, 9]. The denoised void and velocities were verified as preserving the characteristics of the original data.

The outlet feeders from HS10, HS13, and HS14 always had inflows to the outlet header, while the flows in the outlet feeders from HS11 and HS12 reversed direction around 17100 seconds. If an outlet feeder had inflow, a fixed flow boundary condition was set for both phases, in which the void and different phase velocities occur. If an outlet feeder

had outflow, i.e., it becomes an ordinary outlet, fixed pressure was set as the boundary condition.

Achieving consistency among the pressures at different outlets during flow reversal is crucial to predict reasonably correct outflows. This process was complicated by virtue of the fact that the noise in the CATHENA results was strong enough to cause the PHOENICS calculated outflows to fluctuate between positive and negative values. Thus the experimentally derived pressure at the outlet to the boiler and the CATHENA pressures at the outlet feeders were first denoised at very low frequency to capture the true trend of the data. Then a steady-state run at 18200 seconds, around which the system is relatively stable, was conducted. The purpose was to determine the PHOENICS calculated outflows, when using the denoised CATHENA signals as boundary conditions, and compare these with measurement. This permitted the derivation of a pressure offset to apply to the CATHENA pressures, such that valid outflows from feeders HS11 and HS12 would be achieved. As a result, 900 Pa was subtracted from the CATHENA pressure at HS11. This correction was applied during the transient simulation up to 20724 seconds, namely, prior to flow stalling in HS11, when the CATHENA predicted pressure at HS11 dramatically drops. To maintain valid outflow from this point on, a correction of 200 Pa was applied.

5. Results and Discussions

As noted above, the CATHENA predictions reproduced by AECL [4] were used as the boundary conditions at the outlet feeders. During the flow reversal period, when the outlet feeders from HS11 and HS12 actually become an additional two outlets from outlet header #5, the pressure predicted by CATHENA at HS11 was corrected, relative to the experimentally derived pressure at the outlet to boiler #1, to ensure that the experimentally observed flowrates were obtained. Figures 2 and 3 compare the flow rates predicted by PHOENICS at HS11 and HS12 with the measurements, respectively, where “6 Step” and “3 Step” indicate the number of time steps used to cover the transition period from 17124 to 20724 seconds for the time-step independence test. The measurement bands confine the experimental flow rates for almost the entire flow reversal period simulated in this study, except at the beginning when the flows start to reverse, and near the end when the flow in HS11 is stalling. The data bands are shown, rather than actual measurement data, since the flow reversal predicted by CATHENA is about 500 seconds earlier than the test. There are two short duration spikes in the predicted HS12 outflow at the beginning, but they will have a negligible effect on the general conservation of the outflow from the header during the much longer flow reversal period afterwards.

Initially the dead-ended pipe was full of water. The ample volume it provided was once a concern, since its refilling the header with liquid water could aid in forcing the flows in outlet feeders to reverse by increasing the overall liquid level in the outlet header. On the

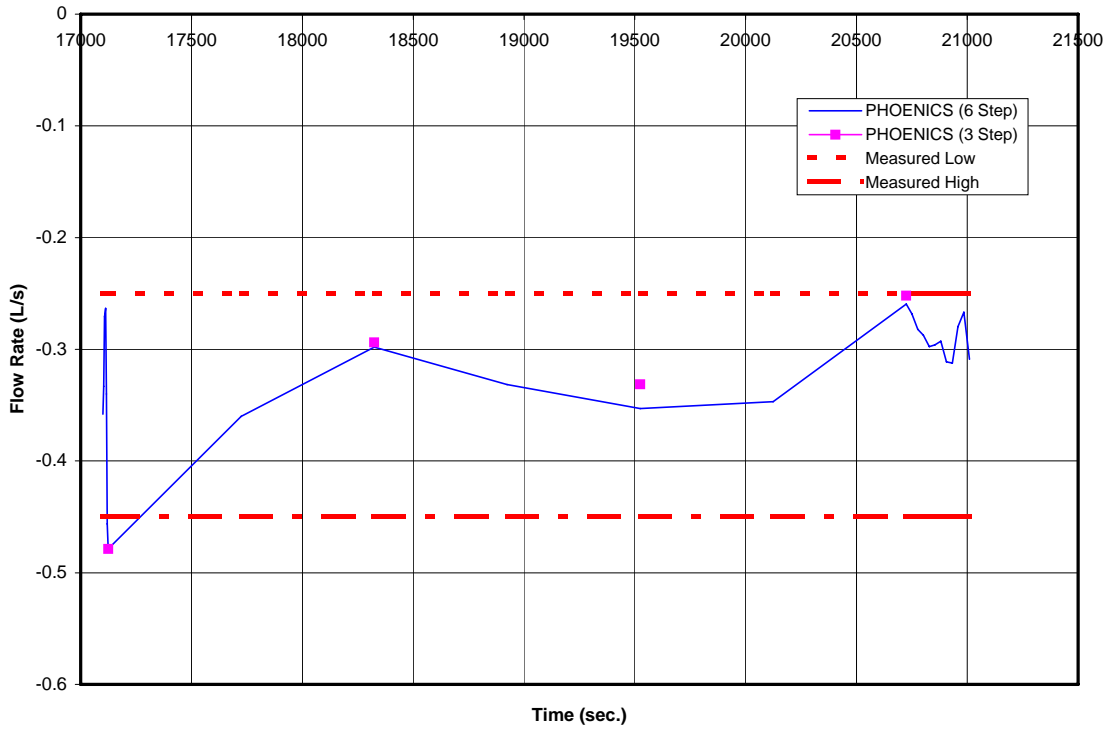


Figure 2. Comparison of flow rates at HS11

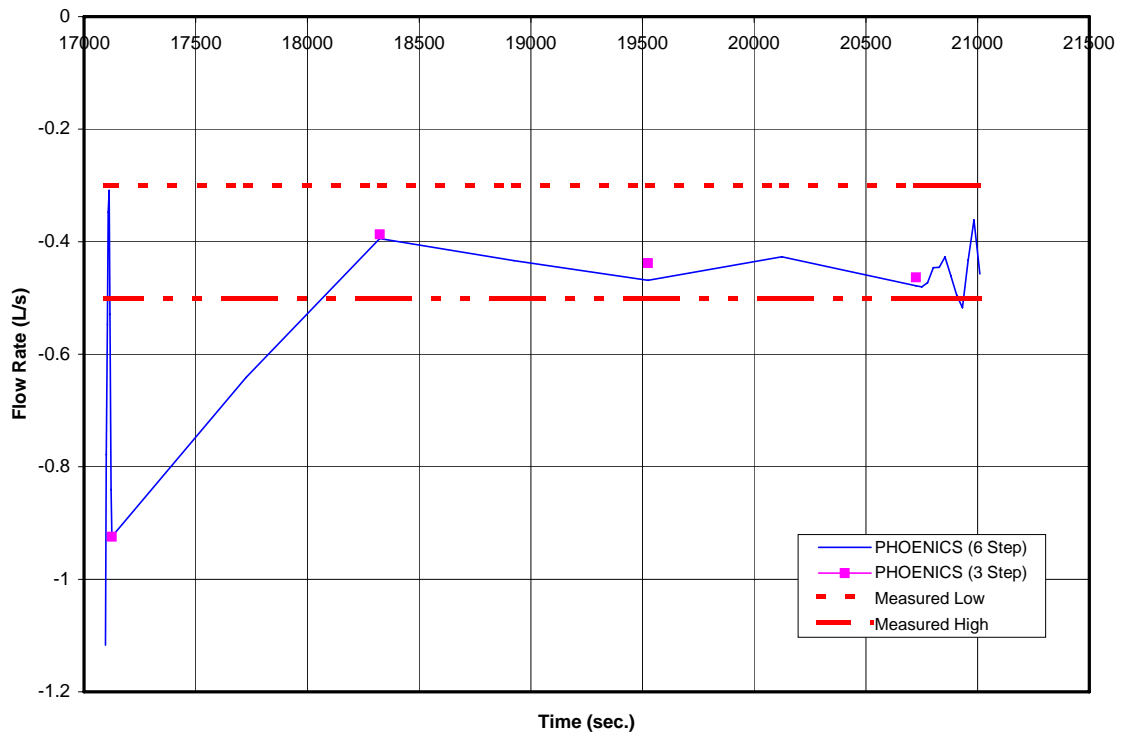


Figure 3. Comparison of flow rates at HS12

other hand, the refilling could also delay the flow stalling once the flow is reversed by maintaining a reasonable liquid level in the header. The transient modelling has, however, found that there is little refilling over the entire simulated time period. Therefore, the dead-end pipe can be removed from the model to save CPU time, if similar work is to be conducted in the future.

Two-phase stratification within the outlet header is shown to exist throughout the transient simulation, as expected. The stratification should be considered along with the discussions that follow.

As observed in Figure 4, the average void within the header rapidly dropped from ~21% at 17044 seconds to ~4% at 17076 seconds, and remained at that low level until after the first flow reversal around 17096 seconds. It then increased to about 25%, and stayed there from about 18000 – 20500 before the FES in HS11 started to heat up at around 20900 seconds. The low average void before flow reversal was due to low incoming velocity and void from the outlet feeders, especially from those of HS10, HS11, and HS12. This led to high liquid levels at the outlet feeder ports for HS11 and HS12, as shown in Figure 5 at 17076 seconds for HS12, where the flow reversal first occurred.

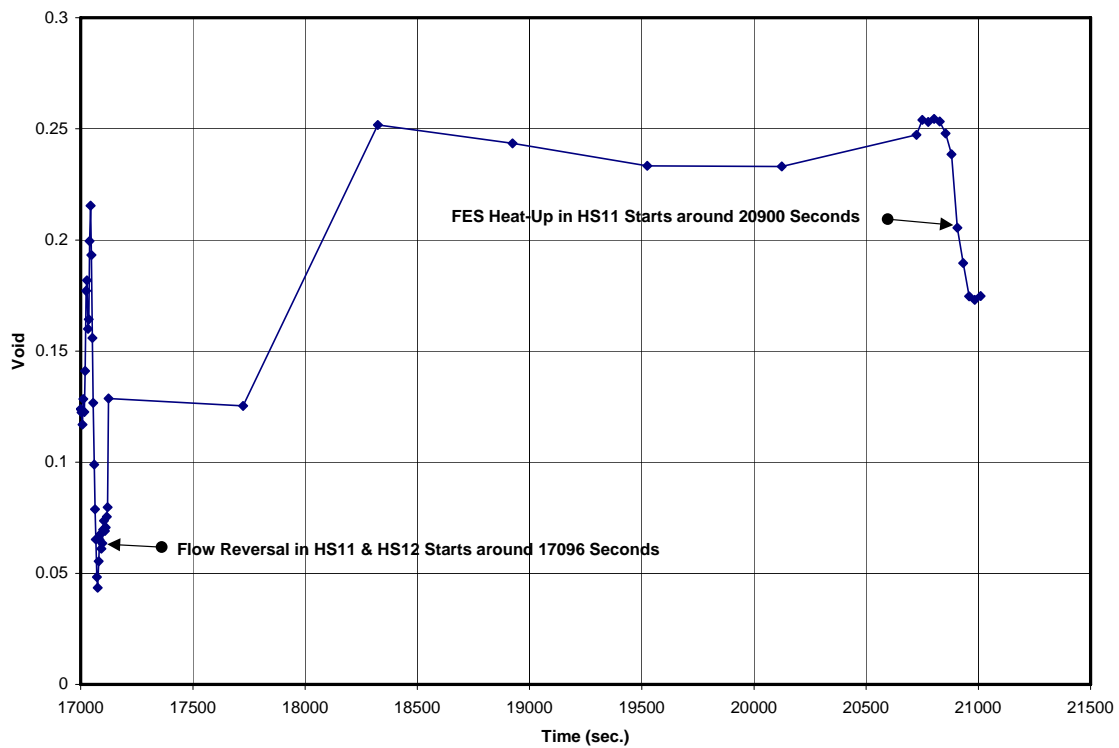


Figure 4. Predicted averaged void within the outlet header #5

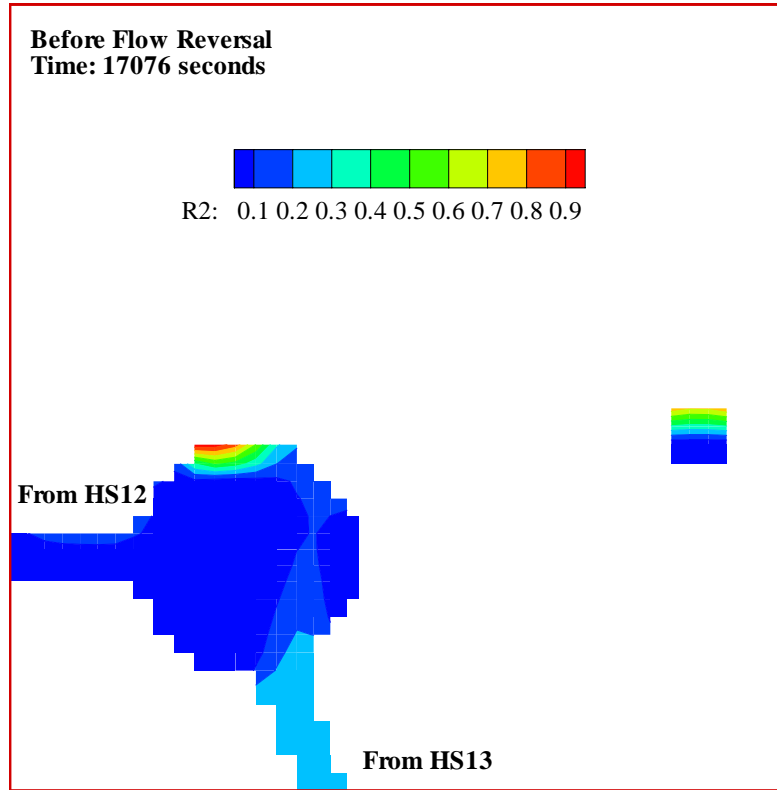


Figure 5. Void distribution at 17076 seconds across the HS12 and HS13 outlet feeder ports

This may have further reduced the incoming flows from HS11 and HS12 and accelerated the occurrence of the flow reversal. The long-lasting high average void prior to FES heat-up in HS11 was, on one hand, due to the sustained drain of the liquid during flow reversal from the HS11 and HS12 outlet feeders, as predictions indicate that the void in the outflows was extremely low. On the other hand, the incoming velocity and void from the outlet feeders of HS10, HS13, and HS14 were high during this period, namely, around 0.6 for void, and between 1 and 2 m/s and 2 and 3 m/s for liquid and steam velocities, respectively. The high average void resulted in low liquid levels at the HS11 and HS12 ports, as depicted at 20750 seconds for HS11, where the FES heat-up occurred (Figure 6). This may have limited the outflow from the HS11 port, possibly leading to flow stalling followed by FES heat-up in HS11.

There is one concern regarding the positions of the outlet feeder ports within the header. The incoming flows from HS10 and HS11 can directly impinge with each other, as do the streams from HS12 and HS13. Since the ports for HS10 and HS11 and for HS12 and HS13 were within the same plane, respectively, along the header axial direction, the jets with higher momentum (sometimes from HS11 and HS13) have deflected their low

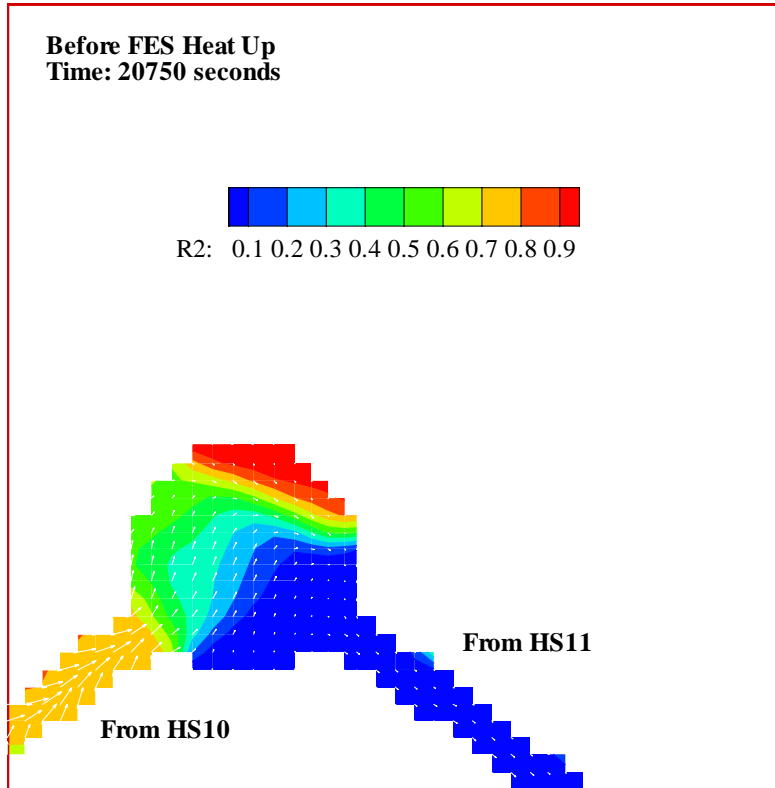


Figure 6. Void and liquid vector distribution at 20750 seconds across the HS10 and HS11 outlet feeder ports

momentum counterparts. While the incoming jet impingement before flow reversal could have facilitated the occurrence of flow reversal, the incoming jet entrainment of the outflow due to the same positioning concern could lead to the flow stalling in HS11. As illustrated in Figure 6 at 20750 seconds, the high momentum jet from HS10 apparently entrained the fluids that otherwise could have flowed out of the header from the HS11 port. Note that the void from HS10 at this time is above 0.6. Subsequently, it dropped to about 0.5, so that the entrainment potential was greater. Also, the predicted outflow from HS11 after this point was higher than the measured flow, since the former remained at about the same level while the flow stalling gradually approached to near zero. Therefore, the entrainment hereafter can be stronger, too, in this context.

There is also a concern about the distribution of the coolant among the outlet feeders. In contrast to the actual CANDU reactor, there are only five outlets feeding into the outlet header in the present geometry. Due to occasional system instability during thermosyphoning, flows can come in from HS13 and HS14 at very high velocity. Figure 7 shows that at 17124 seconds, a jet with very high momentum from HS13 divided the long header with an inner diameter of only 19.4 cm into two parts. Since the outlet feeder

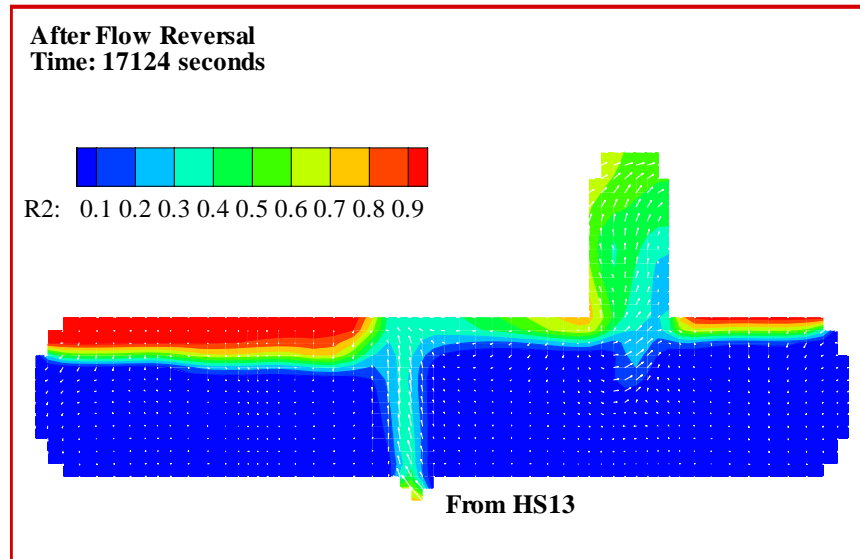


Figure 7. Void and liquid vector distribution at 17124 seconds on the mid-plane of the header

ports for HS10 and HS11 are within the portion farthest from the boiler pipe, the resultant pressurisation in this region could promote flow reversal. The high momentum jet from HS14, on the other hand, might not have posed significant adverse influence on the normal flow condition within the header in this case, since the spacious dead-ended pipe provided a damping effect on the high momentum, as shown in Figure 8 at 17036 seconds.

6. Concluding Remarks

Transient flow conditions within the outlet header #5 of RD-14M, around the occurrence of flow reversal in HS11 and HS12 and FES heat-up in HS11 during test T9308, were numerically analysed. This was performed on the assumption that the CATHENA predictions of void and phase velocities that are reproduced by AECL [4] according to TTR-642 [2] could represent the experimental measurement at the outlet feeders.

It was found that the flow conditions within the header may not be responsible for initiating the flow reversals in the heated sections 11 and 12. The observed high liquid level within the header, the incoming jet impingement with each other, and the incoming jet blocking of the header might have further depressed the already slowed incoming

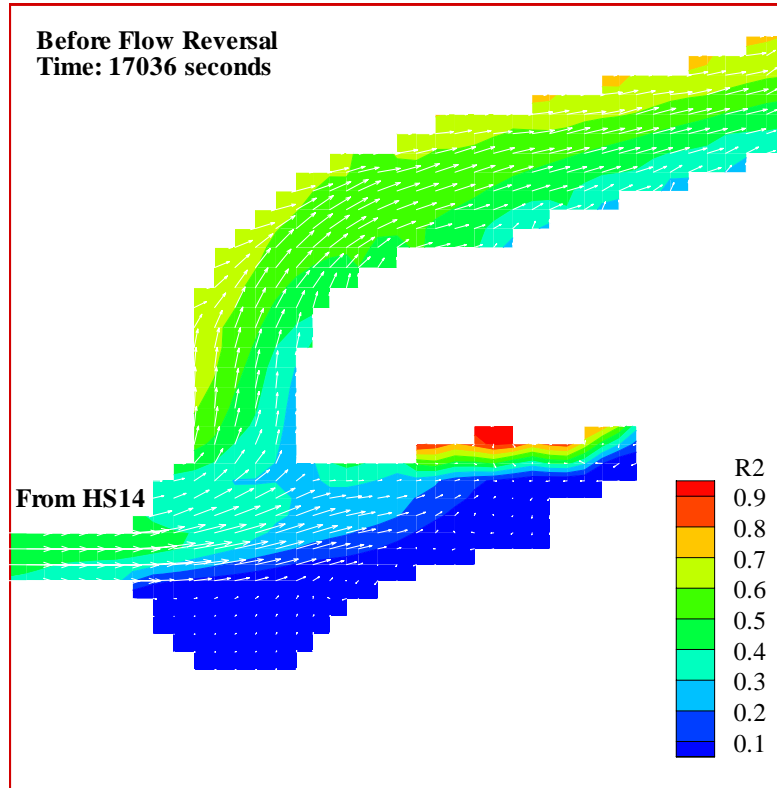


Figure 8. Void and liquid vector distribution at 17036 seconds across the HS14 outlet feeder port

flows from HS11 and HS12 due to system instability before flow reversal occurred. They were not strong enough, however, to force up the original downward liquid flow in the inlet feeders, if the flow of the steam generated in the heated sections is maintained in the desired direction.

It is clear from measurements that the FES heat-up in HS11 is a result of flow stalling in the same channel. The long-lasting low liquid level within the header prior to the FES heat-up, coupled with the fluid entrainment by the HS10 high momentum incoming flow from the region near the HS11 port, could be related to the flow stalling in the HS11 outlet feeder. However, it is also likely that a counter-current steam flow exists in HS11, which blocks the downward liquid flow.

The most significant finding of this preliminary work, however, is believed to be that the scaled nature of the header, along with the presence of only five attached feeders, permits a partitioning of the RD-14M header into pressure/void segments, with associated local effects. Such partitioning is believed to be highly unlikely in the header of a full scale

CANDU, in which the feeders from 95 channels from different regions of the reactor mix along the header length.

References

1. McGee, G.R., et al., RD-14M Facility Description, COG Report, COG-88-42, 1989.
2. Ross, W.E. and Ballyk, J.D., Assessment of CATHENA for Thermosyphoning Applications: Test T9308 Heated Section Simulations, AECL Report, TTR-642, July 1998.
3. Byskal, D., Re: RD-14M Header 5 Model, pers. comm. D. Byskal to W. Thompson, 1 February 1999.
4. Ballyk, J.D., RD-14M Files, pers. comm. J. Ballyk to W. Thompson, 25 January 2000.
5. CHAM, PHOENICS Computational Fluid Dynamics Software ver. 3.2, Concentration, Heat & Momentum Limited, London, UK.
6. CHAM, POLIS for PHOENICS Computational Fluid Dynamics Software ver. 3.2, Concentration, Heat & Momentum Limited, London, UK.
7. PLGS Library, CD-ROM: RD14M04.
8. Atlantic Nuclear Services Ltd., User's Manual for Plant Analysis Workbench (PAW) v. 2.20, October 1999.
9. Lina, J.M. (Atlantic Nuclear Services Limited) and Mayrand, M. (Université de Montréal), Complex Daubechies Wavelets, Applied and Computational Harmonic Analysis, 2 (1995), 219.